

# Structural analysis of the B-doped mesophase pitch-based graphite fibers by Raman spectroscopy

M. Endo, C. Kim, and T. Karaki

*Faculty of Engineering, Shinshu University, 500 Wakasato, Nagano 380, Japan*

T. Tamaki and Y. Nishimura

*Advanced Material Division, Petoka Ltd., Tokyo 102, Japan*

M. J. Matthews and S. D. M. Brown

*Department of Physics, Massachusetts Institute of Technology, Cambridge, Massachusetts 02139*

M. S. Dresselhaus

*Department of Electrical Engineering and Computer Science, Massachusetts Institute of Technology, Cambridge, Massachusetts 02139*

(Received 7 April 1998)

Milled B-doped mesophase pitch-based carbon fibers (mMPCF's) prepared from a melt-blown petroleum mesophase pitch precursor material have been developed for enhanced Li uptake capacity in Li ion batteries. Raman spectroscopy has been used to investigate the structure of graphitized and B-doped mMPCF's using 632.8-nm HeNe laser excitation. The B-doped mMPCF's show a strong Raman peak near  $1330\text{ cm}^{-1}$ , a well-defined peak at  $1620\text{ cm}^{-1}$ , and the disappearance of the second-order  $2660\text{ cm}^{-1}$  band. Furthermore, it is shown that the  $E_{2g2}$  graphite Raman band at  $1580\text{ cm}^{-1}$  is shifted to  $1590\text{ cm}^{-1}$  due to B doping. The appearance of a new weak Raman band in the B-doped mMPCF's near  $1320\text{ cm}^{-1}$  is closely related to the B-C stretching mode in the graphite lattice. These results are associated with the breakdown of the  $k=0$  selection rules by a local distortion of the graphite lattice due to substitutional boron doping. On the basis of the integrated intensity ratio  $R$  of the disorder-induced line near  $1330\text{ cm}^{-1}$  to the Raman line near  $1590\text{ cm}^{-1}$  after 2.66 at. % boron doping, it is suggested that the substitutional boron in the mMPCF's is homogeneously distributed within the graphene layer in the fiber form. The crystallite domain size  $L_a$  parallel and perpendicular to the fiber axis on the surface of the fiber is estimated to be about  $60\text{ \AA}$ , which could correspond to the distance between boron atoms substituted for C atoms in a graphene layer of the fibers.

[S0163-1829(98)08538-5]

## I. INTRODUCTION

Recently, mesophase pitch-based carbon fibers (MPCF's) have been investigated extensively as a functional material in new applications fields, such as for anode materials in Li ion batteries.<sup>1,2</sup> Much effort has been given to the modification of MPCF's for their applications as an anode in Li ion batteries. In particular, B-doped carbonaceous materials are considered as an interesting candidate for practical applications as an anode material for Li ion batteries.<sup>3</sup> It has been shown that boron-doped carbon and graphite display enhanced anode performance, with regard to energy storage capacity and Coulombic efficiency.<sup>3,4</sup> Lowell<sup>5</sup> reported that the maximum amount of substitutional boron in the graphite lattice is at 2.35 at. %, and the B-doped graphite was prepared by the high-temperature reaction at  $2350\text{ }^\circ\text{C}$  of  $\text{B}_4\text{C}$  with natural graphite. Several researchers have also reported on the structure of boron-substituted carbonaceous materials using Raman spectroscopy.<sup>6,7</sup>

Raman spectroscopy has been recognized as one of the most sensitive methods to study the structural properties of carbonaceous materials. Raman spectra provide information on crystalline perfection of graphite-based materials because Raman scattering from perfect crystals is limited to contributions from Raman-active zone-center modes.<sup>8,9</sup> It is well known that the Raman spectrum of single-crystal graphite

and HOPG (highly oriented pyrolytic graphite) in-plane modes with  $E_{2g}$  symmetry consists of a single band at  $1582\text{ cm}^{-1}$  ( $G$  mode,  $E_{2g2}$ ) and another band at  $42\text{ cm}^{-1}$  ( $E_{2g1}$ ), whereas in disordered carbons the Raman spectra show an additional strong band at  $\sim 1360\text{ cm}^{-1}$  ( $D$  mode) and a weak band at  $1620\text{ cm}^{-1}$  ( $D'$  mode), when excited by  $\lambda = 488\text{ nm}$  radiation.<sup>10,11</sup> Simultaneously, the second-order spectra of single-crystal graphite and HOPG show doublet bands at  $2695\text{ cm}^{-1}$  ( $G'_1$  mode) and  $2735\text{ cm}^{-1}$  ( $G'_2$  mode), whereas disordered carbons yield poorly defined peaks at about  $2700\text{ cm}^{-1}$  and  $2900\text{ cm}^{-1}$  ( $D''$  mode).<sup>12</sup> Moreover, the disorder-associated  $D$  mode exhibits a significant excitation-dependent shift from  $1355\text{ cm}^{-1}$  (using the  $514.5\text{ nm}$  Ar-ion laser line) to  $1330\text{ cm}^{-1}$  (using the  $632.8\text{ nm}$  HeNe line), whereas the  $E_{2g2}$  associated mode ( $G$  mode) position is almost independent of changes in excitation frequency.<sup>13</sup> Because of the correlation of disorder with the  $D$  band, Raman scattering is sensitive to changes in structure, and is therefore an important technique to distinguish between ordered and disordered carbon and graphite materials. Also, the longer excitation wavelength could provide new information on the Raman-active bands of disordered carbonaceous materials due to the enhancement of lower frequency peaks.

In the present work, Raman spectroscopy is used to characterize the structure of milled graphitized and B-doped

MPCF's comparatively as prepared from melt-blown petroleum mesophase pitch. These materials are very promising as an anode material in advanced Li ion batteries, since B doping leads to an about 11% increase in discharge capacity.<sup>14</sup> First, the features of the different carbon structures are identified. Also presented here are new structural aspects of graphitized as well as B-doped mMPCF's for use in electrochemical applications. These results could be expected to contribute to developing further applications for carbon fibers.

## II. EXPERIMENT

The milled mesophase pitch-based carbon fibers (mMPCF's) were prepared using a melt-blown method for fiber synthesis from petroleum mesophase pitch.<sup>3</sup> Oxidation of the pitch precursor fibers was performed in air at about 300 °C. The fibers were then milled to be about 50  $\mu\text{m}$  long, and the milling was followed by a carbonization heat treatment at 650 °C. The samples of these materials were subsequently heat treated at 3000 °C in high-purity argon gas (99.999%) for 1 h using a graphite resistance furnace. The boron-doped mMPCF's were prepared by mixing of mMPCF's and 5 wt. %  $\text{B}_4\text{C}$ , and then heat treated to 3000 °C in a flow of high-purity Ar gas (99.999%) for 1 h. The boron content was determined to be 2.4 wt. % (2.66 at. %) by elemental analysis, which might involve the free boron and experimental errors in elemental analysis. The boron doping level is very similar to the maximum solubility of 2.35 at. % reported by Lowell.<sup>5</sup>

An x-ray diffractometer (Rigaku Geigerflex, 30 kV, 10 mA) with a Cu  $K\alpha$  ( $\lambda = 0.15406$  nm) was used to measure the Bragg reflections from graphitized and B-doped mMPCF's, and the lattice parameters  $L_c$  and  $L_a$  of the samples were determined from the widths of the (002) and (110) lines, respectively, as discussed below. Raman scattering experiments were carried out both on the cross section from near the fiber center to the periphery and also on the longitudinal surface with the electric field polarized either parallel or perpendicular to the fiber axis direction. Raman spectra were taken at room temperature under ambient conditions using a Renishaw Image Microscope System 3000 equipped with a charge-coupled device multichannel detector. The Raman instrument was coupled to a standard Olympus microscope and a collection optics system. The excitation source was a 632.8 nm HeNe laser line. The optical power at the sample position was maintained at 25 mW, and no laser annealing effects were observed. The scattered light was collected in a backscattering configuration and the Raman spectra in the range 1000–3000  $\text{cm}^{-1}$  were recorded at a 2.0  $\text{cm}^{-1}$  resolution.

## III. RESULTS AND DISCUSSION

Some properties of graphitized (mMPCF's) and B-doped mMPCF's (B-mMPCF's) used in this study are shown in Table I for comparison. The average interlayer spacing  $d_{002}$ , and the crystallite dimensions  $L_{c(002)}$  and  $L_{a(110)}$  were determined by x-ray measurements using the Bragg and Scherrer formulas, respectively,

$$n\lambda = 2d \sin \theta, \quad L = (K\lambda/\beta \cos \theta),$$

TABLE I. Some properties of graphitized and B-doped mMPCF's studied.

Sample ID	Elemental Analysis (wt. %)				XRD (nm)		
	C	H	N	Diff. <sup>a</sup>	$L_{c(002)}$	$L_{a(110)}$	$d_{002}$
mMPCF's	99.999	0	0	0.001	23	80	0.3367
B-mMPCF's	97.600	0	0	2.400	27	63	0.3355

<sup>a</sup>Difference [We regard the difference value between carbon and 100% as the boron substituted weight (%) in the graphite samples.]

where  $\theta$  is the scattering angle,  $d$  is the interlayer spacing,  $\lambda$  is the wavelength of the x rays used, and  $\beta$  is the half-maximum linewidth in radians. Jeffrey<sup>15</sup> determined that the form factor  $K$  is 0.9 for  $L_c$  and 1.84 for  $L_a$ . These values are used to calculate  $L_{c(002)}$  from the 002 diffraction peak width and  $L_{a(110)}$  from the 110 peak width in Scherrer's equation. B-doped mMPCF's show a growth in crystallite thickness,  $L_{c(002)}$ , and a decrease in interlayer spacing  $d_{002}$ , and crystallite width,  $L_{a(110)}$ , relative to that of undoped mMPCF's (see Fig. 1). The decrease in  $d_{002}$  and  $L_{a(110)}$  may be related to the depleted  $\pi$  electrons between graphite layers, which leads to a shorter interlayer distance, as well as to lowering the density of  $\pi$  electrons in the graphite layers because of the lower valence state of boron.<sup>16</sup> This result could be due to the presence of substitutional boron in the graphite layer of mMPCF's, and this boron substitution results in bringing adjacent planes closer together, yielding a contraction of the structure along the  $c$  axis, as observed in general.<sup>6</sup> Thus, the addition of boron can lead to an enhancement of the graphene edge growth. On the other hand, the crystallite width of the B-doped mMPCF's decreases by about 20% relative to that of undoped pristine mMPCF's. It should be noted that such changes of crystallite geometry due to B doping induce a larger crystallite thickness and a smaller crystallite width in the fiber form.

Figure 2 shows the first- and second-order Raman spectra of the graphitized and B-doped mMPCF's, measured with the incident laser radiation on the fiber cross section close to

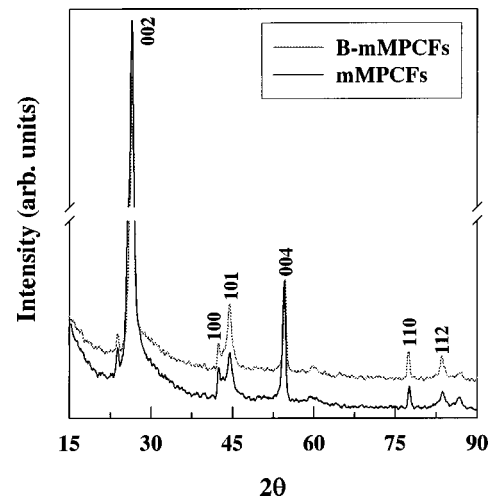


FIG. 1. X-ray diffraction profiles of mMPCF's and B-doped mMPCF's heat treated at 3000 °C. The peaks are labeled by the Miller indices.

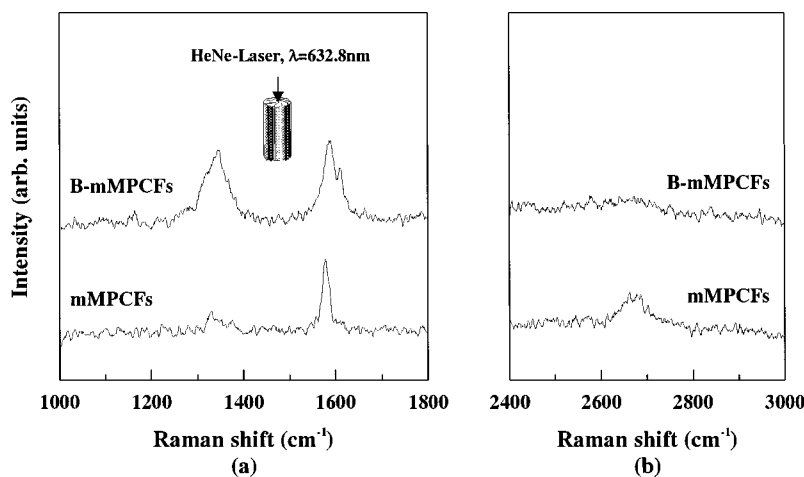


FIG. 2. The first- (a) and second-order (b) Raman spectra of the cross section of mMPCF's and B-doped mMPCF's.

the fiber center. The B-doped mMPCF's show a large increase in the intensity of the  $1330\text{ cm}^{-1}$  ( $D$  band) and a slight decrease in the  $1580\text{ cm}^{-1}$  ( $G$  band) band compared to that in a sample of undoped mMPCF's. In particular, the Raman features at  $1620\text{ cm}^{-1}$  and  $2660\text{ cm}^{-1}$  ( $G'$  band) are, respectively, increased and decreased for the B-doped mMPCF's, when compared to the undoped mMPCF's. The cross section of the undoped mMPCF's shows peaks corresponding to the line near  $2660\text{ cm}^{-1}$  and also a very weak peak at  $1620\text{ cm}^{-1}$  ( $D'$  band). The additional feature near  $1620\text{ cm}^{-1}$  corresponds to a maximum in the phonon density of states and exhibits a behavior similar to that of the  $1330\text{ cm}^{-1}$  disorder-induced line<sup>7-9</sup> with regard to its correlation to disorder. In comparison, the B-doped mMPCF's show a strong Raman peak near  $1330\text{ cm}^{-1}$ , a well-defined peak at  $1620\text{ cm}^{-1}$ , and a decreased intensity for the  $2660\text{ cm}^{-1}$  feature. The features near  $1330$  and  $1620\text{ cm}^{-1}$  might be associated with the local structural distortion in the graphitic lattice due to boron doping, thereby increasing the  $D$  and  $D'$  band intensities.<sup>6</sup> Furthermore, the  $1330\text{ cm}^{-1}$  mode for the B-doped mMPCF's is thought to arise from scattering from nonzone center phonons, which become Raman active because of a loss of transitional symmetry.<sup>11</sup> These results are also corroborated by the position of the  $G'$  overtone at  $2660\text{ cm}^{-1}$  ( $2 \times 1330\text{ cm}^{-1}$ ) that is present in the second-order spectrum of the undoped mMPCF's. The Raman intensity in the  $D$  band and the upshifted  $G$  band have been related to the relaxation of the  $k=0$  selection rule,<sup>6,8,11</sup> and the disorder-induced scattering is enhanced in the case of boron-doped mMPCF's. This phenomenon was associated with a larger force constant for carbon-carbon bonds within the layer planes and the crystal imperfection due to the formation of carbon-boron bonds.

In particular, Raman spectroscopy provides very important information on the microstructure and crystalline ordering in carbon materials in terms of the various spectral parameters, such as intensity, peak position, line shape, and bandwidth. For example, Tuinstra and Koenig<sup>11</sup> used the relative ratio ( $R$ ) of the integrated intensity for the  $D$  and  $G$  lines to provide a measure of  $L_a$ . More recently, Knight and White<sup>17</sup> developed an empirical formula that relates  $R$  to the crystallite domain size  $L_a$  of graphite as  $L_a = (44/R)$  for spectra taken at  $514.5\text{ nm}$ . Both the peak position and bandwidth of  $G$  and  $D$  lines are sensitive to  $L_a$ . The Raman-

derived structural parameters of graphitized and B-doped mMPCF's are also added to Table II.

Figures 3 and 4 show the first- and second-order Raman spectra of the graphitized and B-doped samples for a longitudinal surface, with light polarized parallel ( $E_{\parallel}$ ) and perpendicular ( $E_{\perp}$ ) to the fiber axis, respectively. In both samples, the longitudinal surface in the perpendicular direction ( $E_{\perp}$ ) shows strong peaks near  $1330\text{ cm}^{-1}$  ( $D$  band), and weak peaks near  $1580\text{ cm}^{-1}$  ( $G$  band) and  $2660\text{ cm}^{-1}$  ( $G'$  band) when compared to the parallel direction ( $E_{\parallel}$ ), and this decrease in intensity may be associated with a decrease in the graphite domain size. We have performed a line-shape-fitting analysis of the  $D$  band in the spectra of graphitized and B-doped mMPCF's using Lorentzian functions for the constituent components of the Raman lines. Furthermore, the Raman spectrum for the B-doped mMPCF's clearly shows a shoulder peak at about  $1320\text{ cm}^{-1}$  when compared with undoped mMPCF's, as demonstrated in Fig. 5. The shoulder peak at  $1320\text{ cm}^{-1}$  may be due to the B-C vibrational mode in the graphite lattice, which results from the addition of boron, as well as a different phonon frequency of the  $sp^2$ -bonded crystallite present in B-doped mMPCF's. From the above results, we interpret the  $D$  and  $D'$  peaks associated with the B-C vibration to be influenced by the smaller number of electrons in boron, which causes a redistribution of the  $\pi$  bonding and a difference in the bond length of B-doped neighboring carbons compared with the ordinary C-C vibrations in mMPCF's. Consequently, B-doped mMPCF's presumably give rise to new electron states in an acceptor level. Furthermore, B-doped mMPCF's show a new shoulder peak at  $1320\text{ cm}^{-1}$  which provides good evidence for two components of the Raman mode in graphite, where one of the components is induced by disorder and is associated with a localized B-C vibrational mode. On the other hand, we have not detected a shoulder peak due to the B-C vibrational mode of B-doped mMPCF's using the  $514.5\text{-nm}$  Ar-ion laser line shown in Fig. 6. These results may be related to the fact that the  $632.8\text{-nm}$  HeNe laser line provides new information on the disorder-induced band due to the enhancement of the  $D$  peak that is expected at longer wavelengths.<sup>13</sup>

Table II shows the peak position, integrated intensity ratio  $R(I_D/I_G)$ , bandwidth  $\omega_{1/2}$ , and calculated domain size  $L_a$  (Ref. 17) of the present samples, where  $R(I_D/I_G)$  and  $L_a$  are

TABLE II. Raman spectroscopic parameters obtained after curve fitting the experimental spectra by using Lorentzian fits to the Raman lines.

Sample I.D.	Peak position $\nu$ ( $\text{cm}^{-1}$ )		Bandwidth $\omega_{1/2}$ ( $\text{cm}^{-1}$ )		$R(I_D/I_G)$	$L_a(\text{\AA})^{17}$	
	$\lambda = 514.5$ nm	$\lambda = 632.8$ nm	$\lambda = 514.5$ nm	$\lambda = 632.8$ nm			
mMPCF's	$E\parallel$	1355	1335	21	29	0.09	448
		1580	1580	10	9		
		2666	2666	39	39		
	$E\perp$	1355	1334	25	21	0.17	258
		1580	1582	10	10		
		2665	2665	34	34		
B-mMPCF's	$E\parallel$	1365	1324	25	8	0.77	57
		1589	1345	14	19		
		1618	1590	6	14		
	$E\perp$	1365	1310	25	1	0.76	57
		1591	1343	15	24		
		1621	1587	5	12		
		1613	1613	6	6		

obtained from the measurements at 514.5 nm. It is interesting to note that  $L_a$  along the fiber axis is about two times larger along the direction parallel ( $E\parallel$ ) to the fiber axis, as compared to the ribbons of the graphene layers arranged on the fiber surface perpendicular ( $E\perp$ ) to fiber axis. On the other hand, for the B-doped mMPCF's, the crystallite domain size  $L_a$  parallel and perpendicular to the fiber axis is the same for

the two directions and is estimated at about 6 nm, which is very close to the distance between boron atoms substituted for C atoms in the graphite layer planes. We thus conclude that the boron is homogeneously distributed within the graphite layer planes of the boron-doped mMPCF sample. On the other hand, x-ray results indicate that the B-doped mMPCF's have  $L_a$  values about 63 nm. In these samples the

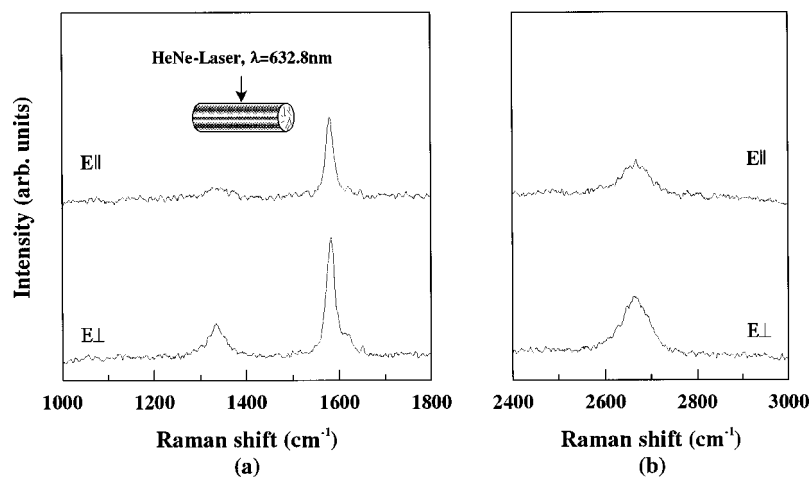


FIG. 3. The first- (a) and second-order (b) Raman spectra taken from the longitudinal surface in a direction parallel ( $E\parallel$ ) and perpendicular ( $E\perp$ ) to the fiber axis of the mMPCF's.

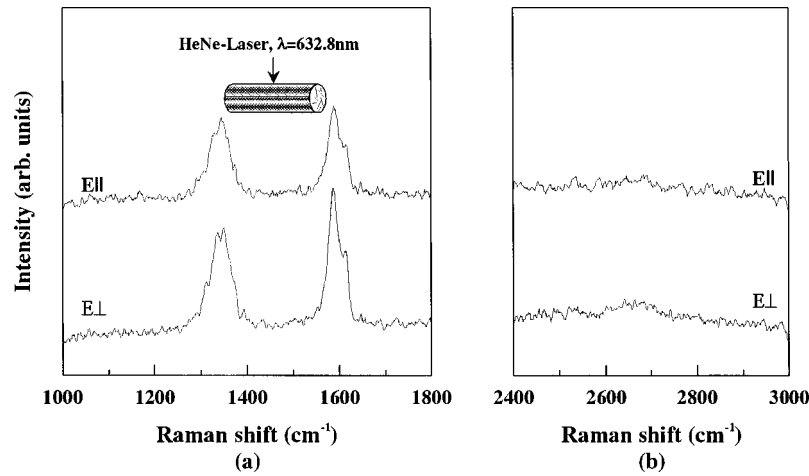


FIG. 4. The first- (a) and second-order (b) Raman spectra taken from the longitudinal surface in a direction parallel ( $E_{||}$ ) and perpendicular ( $E_{\perp}$ ) to the fiber axis of the B-doped mMPCF's.

x-ray results provide an estimate of the dimensions of the relatively flat portions of the crystallites.<sup>6</sup> However, Raman scattering is very sensitive to structural defects present in graphitized and B-doped mMPCF's.

Figure 7 shows a schematic model of a graphite layer plane in which substituted B atoms show different bond lengths between the B-C and C-C bonds. Data from a Silicon Graphics simulation are shown in this figure.

#### IV. CONCLUSIONS

Graphitized and B-doped mMPCF's have been investigated and characterized mainly by Raman scattering, and the results obtained are compared with additional data obtained by the x-ray diffraction (XRD) technique. The effect of B doping enhances the growth of the crystallite thickness,  $L_{c(002)}$ , but decreases the crystallite width,  $L_a$ , of the host mMPCF's, as indicated by XRD and Raman scattering results. In the present study, B-doped mMPCF's presumably give rise to a new electronic acceptor state. The appearance of a new Raman band at  $1320\text{ cm}^{-1}$  in the B-doped

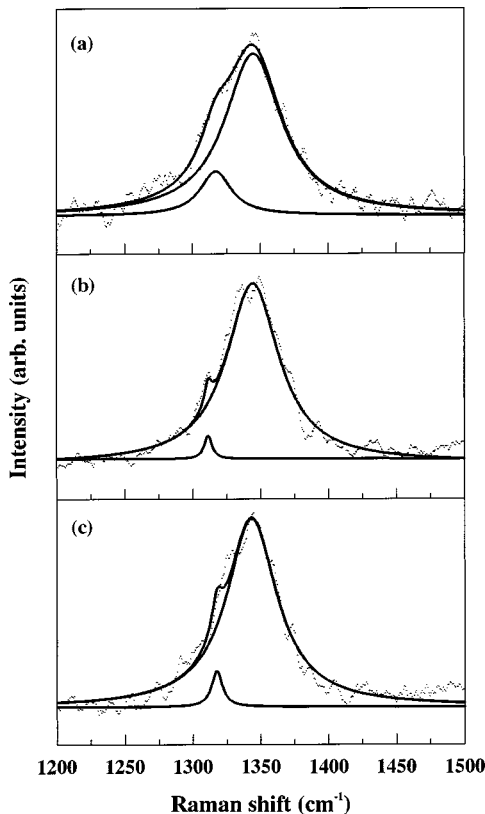


FIG. 5. Line-shape fitting of the  $D$  band for the B-doped mMPCF's; (a) cross section, (b) parallel ( $E_{||}$ ) to the fiber axis, and (c) perpendicular ( $E_{\perp}$ ) to the fiber axis. The Lorentzian components and the final curve are a continuous line for each spectrum.

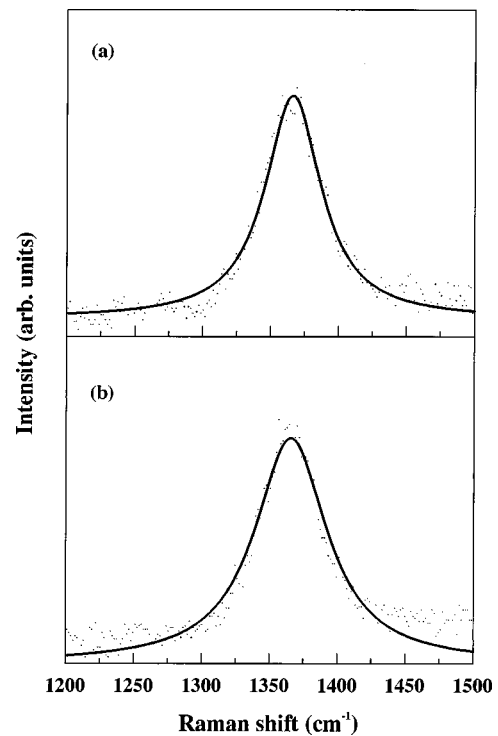


FIG. 6. Line-shape fitting of the  $D$  band for the B-doped mMPCF's excited at  $514.5\text{ nm}$  Ar-ion laser line; (a) parallel ( $E_{||}$ ) to the fiber axis and (b) perpendicular ( $E_{\perp}$ ) to the fiber axis. The Lorentzian components and the final curve are a continuous line for each spectrum.

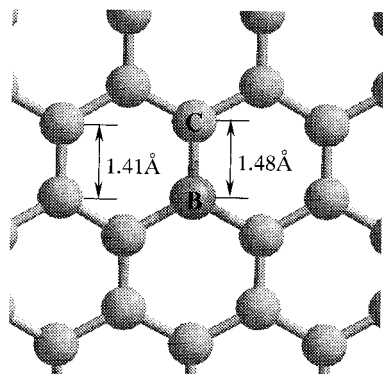


FIG. 7. Schematic representation of a graphene plane of the 2.66 at % B-doped mMPCF's. The difference in bond length between a B-C and C-C bond is indicated. Data from a Silicon Graphics simulation are shown.

mMPCF's is closely related to the B-C vibrational mode for B in substitutional sites in the graphite lattice. An increase in the intensity of the *D* band and the appearance of the *D'*

band in the B-doped mMPCF's is associated with the breakdown of the  $k=0$  selection rules by a local distortion of the graphite lattice due to boron doping. Finally, the integrated intensity, *R*, for boron-doped mMPCF's as a function of distance parallel ( $\parallel$ ) and perpendicular ( $\perp$ ) to the fiber axis shows that B is homogeneously distributed within the graphite layer planes of the fiber surfaces. On the other hand, the crystallite domain size  $L_a$  parallel and perpendicular to the fiber axis is about 6 nm, which is very close to the average distance between boron atoms that are substituted for C atoms in the graphene layer planes.

These results may be important for the use of boron as an additive to mMPCF's for use in applications such as for anode materials in Li ion batteries.

#### ACKNOWLEDGMENTS

The M.I.T. authors acknowledge support from NSF Grant No. DMR 98-04734. The authors wish to thank Professor Marcos Pimenta and Dr. G. Dresselhaus for helpful discussions.

- <sup>1</sup>N. Takami, A. Satoh, M. Hara, and T. Ohsaki, *J. Electrochem. Soc.* **142**, 2564 (1995).
- <sup>2</sup>M. Endo, Y. Nishimura, T. Takahashi, K. Takeuchi, and M. S. Dresselhaus, *J. Phys. Chem. Solids* **57**, 725 (1996).
- <sup>3</sup>Y. Nishimura, T. Takahashi, T. Tamaki, M. Endo, and M. S. Dresselhaus, *Tanso* **172**, 89 (1996).
- <sup>4</sup>B. M. Way and J. R. Dahn, *J. Electrochem. Soc.* **141**, 907 (1994).
- <sup>5</sup>C. E. Lowell, *J. Am. Ceram. Soc.* **50**, 142 (1967).
- <sup>6</sup>T. Hagio, M. Nakamizo, and K. Kobayashi, *Carbon* **27**, 259 (1989).
- <sup>7</sup>J. G. Naeini, B. M. Way, J. R. Dahn, and J. C. Irwin, *Phys. Rev. B* **54**, 144 (1996).
- <sup>8</sup>T. C. Chieu, M. S. Dresselhaus, and M. Endo, *Phys. Rev. B* **26**, 5867 (1982).
- <sup>9</sup>M. S. Dresselhaus and G. Dresselhaus, in *Light Scattering in Solids III*, edited by M. Cardona and G. Guntherodt, Topics in Applied Physics Vol. 51 (Springer-Verlag, Berlin, 1982), p. 3.
- <sup>10</sup>M. S. Dresselhaus, G. Dresselhaus, K. Sugihara, I. L. Spain, and H. A. Goldberg, in *Graphite Fibers and Filaments*, Springer Series in Materials Science Vol. 5 (Springer-Verlag, Berlin, 1988).
- <sup>11</sup>F. Tuinstra and J. L. Koenig, *J. Chem. Phys.* **53**, 1126 (1970).
- <sup>12</sup>R. P. Vidano, D. B. Fischbach, L. J. Willis, and L. J. Loehr, *Solid State Commun.* **39**, 341 (1981).
- <sup>13</sup>M. Endo, C. Kim, M. J. Matthews, and M. S. Dresselhaus (unpublished).
- <sup>14</sup>M. Endo, C. Kim, M. J. Matthews, and M. S. Dresselhaus (unpublished).
- <sup>15</sup>J. W. Jeffrey, *Methods in X-ray Crystallography* (Academic, London, 1971), p. 83.
- <sup>16</sup>H. M. Murty, D. L. Biederman, and E. A. Heintz, *Fuel* **56**, 305 (1977).
- <sup>17</sup>D. S. Knight and W. B. White, *J. Mater. Res.* **4**, 385 (1989).